Hindawi
Mathematical Problems in Engineering
Volume 2021, Article ID 9059722, 12 pages
https://doi.org/10.1155/2021/9059722

Research Article

Multiresponse Particle Swarm Optimization of Wire-Electro-Discharge Machining Parameters of Nitinol Alloys

Mohammed Yunus and Mohammad S. Alsoufi

Department of Mechanical Engineering, College of Engineering and Islamic Architecture, Umm Al-Qura University, Makkah, Saudi Arabia

Correspondence should be addressed to Mohammed Yunus; myhasan@uqu.edu.sa

Received 7 August 2021; Revised 19 October 2021; Accepted 6 November 2021; Published 8 December 2021

Academic Editor: Yong Zhang

The conventional process of machining of nitinol alloy which possesses excess strain hardening and low thermal conductivity makes a complex process that leads to extensive wear on the tool and inadequate surface quality. Wire-electro-discharge machining (WEDM) is widely accepted for machining this alloy involving various input factors, namely, P (pulse-on-duration), Q (pulse-off-duration), C, (maximum-current), and V (voltage). Using the PSO (particle swarm optimization) method, the effect of WEDM process factors on multiresponses such as MRR (metal removal rate) and SR (surface roughness) has been investigated. ANOVA was used to create a relationship model between input factors and response characteristics, which was then optimized using response surface methods (RSM). ANOVA revealed that variables A and C are the most significant. When investigated individually, the influence of WEDM process parameters on SR and MRR is contradictory, as no response provides the best process quality. To find the optimal ideal condition for decreasing SR and maximizing MRR, the MOOPSO approach was used. $P = 25.47051\ \mu$s, $Q = 10.84998\ \mu$s, $C = 2.026317$ A, and $V = 49.50757$ volts were used to calculate the optimal universal solution for machining characteristics ($MRR_{max} = 3.536791\ mm^3/min$ and $SR_{min} = 1.822372\ \mu$m). PSO enhanced MRR and SR for every optimal combination of variables, according to the findings. Based on the findings, a wide range of optimal settings for achieving maximum MRR and minimum SR are given, depending on the product requirements.

1. Introduction

The current state of science and technology necessitates the use of modern materials that are both strong (greater strength) and lightweight (low density). Various alloys are available, particularly those that combine nickel and titanium. Nitinol alloy has long been regarded as one of the most advantageous metals with the desired properties. Shape remembering effect, pseudoadaptability, creep, and corrosion resistant, among other features, are enhanced by adding other blending materials such as Cu, which improves phase shifting temperature levels, sudden reaction to stimulation, and cyclic and vibration damping characteristics. These alloys are unique metallic alloys that are used primarily in the aerospace and automobile industries, as well as in the medical and dental disciplines [1]. Apart from the aforementioned principal fields, they are used in couplers, sealing, simulators, turbine components, scramjet combusting chambers, and so on. Traditional machining procedures on these alloys with a good surface finish to a higher degree of precision for achieving their excellent features are difficult, time-consuming, and costly to implement. Advanced machining plays an important role in gauging alloy properties, reducing labor, lowering production costs, and speeding up and simplifying the process. Strain hardening in nickel and titanium-based alloys, super and shape memory alloys, and other low thermal conductivity alloys are one of their most notable characteristics, as it makes fixed machining processes such as turning, drilling, boring, and milling extremely difficult, as well as causing excessive tool wear and chip sticking [2].

Various advanced machining processes such as ECM (electro-chemical), EDM (electro-discharge), AJM (abrasive-

jet), WEDM (wire-electro-discharge), laser, and hybrid type have proven to be the most adaptable nonconventional machining procedures to hard metals and their alloys in any proportions forming different alloys. WEDM is only affected by breakdown voltage because the wire (made of Cu, brass, Mo, Al, and graphite) is bolstered through the work piece [3]. Because of its high melting point temperature, graphite wire has a higher material removal rate (MRR) than Cu wire, which improves hardness due to titanium carbide formation on the surface, but aluminum wire has a superior surface finish. WEDM's high-temperature technique results in reformed and dampened surfaces that generate residual tensile stresses that cause rupture [4, 5]. Even with constant pulse energy, the surfaces created with short and long discharge current pulses had the same surface roughness, but the distribution of surface finish was found to be different [6]. The response properties (MRR and SR) of shape memory alloy (Ti50Ni42.4Cu7.6) on input factors were explored. When increasing MRR, a combination of low maximum-current (C) and instant pulse-on-duration (P) is more effective than decreasing SR with a high amount of pulse-on-duration [7]. When milling the Ti50Ni49Co1 surface of SMA, the effect of WEDM factors results in poor surface quality at higher P values and a rich surface finish at high speeds [8]. The desirability approach was used to model and optimize WEDM factors of nickel-based superalloys using response surface methodology (RSM). Taguchi technique optimized the MRR, wear, and friction characteristics of trials conducted on Nimonic-80A utilizing WEDM process parameters individually [9]. RSM optimization of SR outputs was carried out, as well as measurement variation of the WEDM process in pure titanium [10, 11].

For handling the intricacy in tackling regular manufacturing optimization issues, the fuzzy controller [12, 13] was suggested, together with its magnificent economical algorithm. However, a meta-analysis showed that there have been no systematic investigations of the input parameters influencing the surface finish and MRR of nitinol (nickel-titanium) alloy using the WEDM method. As a result, the focus of this research is on determining the impact of input variables such as P, Q, C, and V on the machining characteristics of nitinol alloys (MRR and SR). As a result, the current study used CCD standards to construct an experiment to determine the combined impact of factors on the response characteristics of nitinol alloy consuming electrode wire composed of "molybdenum." As a result, significant regression models were created using RSM to investigate the influence of P, Q, C, and V on responses. Optimization is the process of finding the best possible set of elements for maximizing or limiting responses [14]. In previous work for single/multiple answers, Taguchi design, RSM, and the grey relation technique were used to optimize the input variables of WEDM and many other processes. Such strategies are appropriate for single-response optimization, but not for multifactor multiobjective optimization, as their results contradict closing statements [15]. For the first time, Kennedy and Eberhart proposed the PSO technique in 1995 as a tool for translating evolutionary procedures to the optimization of performance attributes [16]. After recognizing the actions of ecological swarm birds returning to settle back, which were found in different categories of flying creatures, the PSO method was utilized to solve trustworthy nonlinear update problems [17]. PSO generates top score measures and a consistent mix of factors in a short estimation time [18]. Numerous engineers/researchers recognize the PSO system's ability to execute the top score of the process as a productive decision over many challenges, particularly when managing multiple-goal updating matters [19].

Advanced and evolving procedures attain success in solving multidimensional objectives with several confined targets. One of them is the PSO approach (stochastic optimization) which uses a population of random solutions to find the best one from the numerous generations created by the starting population, analogous to bird flock management. As a statistical search method, it falls under the genre of evolution algorithms. Furthermore, the PSO is being extended to cope with multiobjective optimization (MOO) issues, and PSO techniques are simple to apply because of their basic mathematical and logical operators [20]. Based on the combined performance in regionalized self-prepared structures, swarm information is regarded a genetic and artificial intelligence. A self-adaption technique based on entropy/nature guidelines for regulating algorithmic parameters from both the population and every inherited place as the answer for evaluating algorithmic state is vital within a genetic algorithm's performance. As a result, variables are regulated in accordance with algorithmic status and nature rules to avoid issues such as early growth and nonconverged particular genes while evaluating their status and tracking their development. Furthermore, it maintains solutions of reasonable quality while also increasing the likelihood of poor-quality solutions varying. The proposed technique has been shown to work for a variety of combinational optimization problems [21].

Binary-differential-evolution with self-learning and the unique three proposed operatives to improve their performance are known as multiresponse attribute selection practice. (1) Built one-bit refining search operatives improved self-taught ability; (2) competent nondominated-sorting operative (NSGA) with crowding-distance (CD) reduces the estimation difficulties of the selection operator in the distinction evolution; and (3) competent nondominated-sorting operative (NSGA) with crowding-distance (CD) reduces estimation difficulties of the selection operator in the distinction evolution. The expected system is more viable than colony-based feature selection algorithms, according to trial findings evaluated on a series of community statistics in attaining a balance between limited modification and global investigation [22]. The NSGA-III can be used to break one of the attribute selection's (AS) primary challenges in real-world applications: lost information. To deal with missing data, the mean imputation method is used. The attribute subgroups were analyzed in the trials using a classifier called k-nearest-neighbours (K-NN). The results of the trials show that the expected additional-objective standard combined with NSGA-III has effectively handled the problem [23]. In high-dimensional data, advanced AS algorithms must deal with dimensionality concerns. A divide-and-conquer strategy is used in an adjustable-size cooperative coprogressive PSO process. To begin, an AS space division

approach is required to identify significant qualities at a tiny estimation figure and to maintain an appropriate size of each subswarm when analyzing particles. Furthermore, particle removal methods take into account fitness-driven binary grouping as well as particle development and crossover to ensure quality. The proposed approach can provide good AS with high dimensionality, according to experimental data [24]. Machining of nickel and titanium (shape memory alloy) from wire EDM using ANOVA empirical models constructed to account for factors affecting MRR and Ra. For optimization, the NSGA-II ranking and CD were used. The MRR and Ra were improved, and the formation of cracks, lumps, and deposited films was reduced significantly [25].

Nitinol alloy's excellent surface quality and high metal removal rate are a fascinating topic in the realm of manufacturing. The amount of research on WEDM machining is limited. There is currently no study being done on the use of PSO for multiple objectives of the nitinol alloy WEDM technique. In this case, the primary research focus is on determining the impact of various parameters on machining characteristics (SR and MRR). The fitness function to optimize responses was adjusted in the mathematical model form using a series of strategic trials, and the importance of it in the form of the RSM model was tested using ANOVA. Furthermore, a multioutput/objective PSO is used to find the top-scored optimum set of factors for maximizing and minimizing the MRR and SR, respectively, with a genetic algorithm and the Pareto font. Using a multioutput genetic algorithm-based PSO, the optimum setup of WEDM process factors was obtained, and the PSO performances of Pareto front solutions were compared and confirmed.

2. Materials and Methods

WEDM was used to prepare workpieces composed of nitinol alloy (nickel-titanium alloy), a commercially accessible material. The construction of numerical models is crucial in the manufacturing process if parts are to be developed quickly and at a lowest machining cost. A realistic model based on RSM can establish a compromise between input elements and responses [12]. The notable correlation between input elements and outcome is expressed as follows in RSM [26]:

$$Z = h\left(a_1; a_2; a_3; \ldots; a_n\right) + \text{error}, \tag{1}$$

where Z is the output characteristic to be optimized, and h is the objective function, which includes both dependent and independent factors a_1, a_2, a_3, …, a_n, as well as error correction. The Taguchi design approach was used to optimize WEDM factors involved in the machining of an aluminum alloy 5754 produced by friction-stir-welding for experimentation planning in an orthogonal array format to take all conceivable various combinations of variables and their levels [27]. Taguchi parametric design and RSM were used to increase the quality and accuracy of the WEDM process. Face-centered composite design (CCD) was utilized to construct mathematical models for the MRR and SR, as well as to explore the influence of factors on accuracy. RSM appears to be an appropriate strategy for studying and optimizing input factors. This strategy improves product authority as well as efficiency [9, 10, 28]. Pulse-on-duration (P), pulse-off-duration (Q), maximum-current (C), and voltage (V) are the process parameters that have a substantial impact on MRR and SR responses. Table 1 outlines the different ranges of process factors.

The fitness function necessary for the PSO technique will be developed using a mathematical model based on RSM. The MATLAB optimization toolbox will use the Pareto front solver to accomplish multiobject optimization with genetic algorithm in PSO.

2.1. Experimental Details. All of the trials on nitinol parts using CNC wire cut EDM employed 0.2 mm diameter molybdenum (Mo) wire as the electrode material. When it comes to making complex geometries parts for aerospace and missiles, Mo wire has a number of benefits, including a high melting temperature and ultimate strength. To use deionized water as a dielectric liquid, care must be taken with the wire diameter and the pressure of the deionized water, which should be kept constant at roughly 2.6 kg/cm^2. Table 2 lists the trials that were collected to determine the CCD full percentage for all factor combinations that occurred at higher (3) and lower (1) levels, i.e., two levels and multiresponses (MRR and SR) of the WEDM process.

$$\text{MRR}\left(\text{mm}^3/\text{min}\right) = \text{volume of material removed} \cdot \left(\frac{\text{length} * \text{width} * \text{depth of cut}}{\text{machining time}}\right), \tag{2}$$

where width of cut in mm = (2 × clearance) + wire diameter.

Surface roughness is measured with a surface roughness tester (Taylor Hobson profilometer) at three separate points on the surface, with the average value displayed in micrometres.

2.2. Multiobjective Optimization Using PSO. Every particle in the group possesses velocity $v_{j(f)}$ with which it can flee into the illustration region and is described by a velocity $v_{j(f)}$ and a position $x_{j(f)}$ vector. The numerous input factors in the optimization process well express their components. Modifications to the particle's location are made using the particle's former position data and present velocity. Thus,

$$\begin{aligned} V_{j(f+1)} &= V_{j(f)} + c_1 \text{rand}_1\left(P_{\text{best}} j - X_{j(f)}\right) \\ &\quad + c_2 \text{rand}_2\left(G_{\text{best}j} - X_{j(f)}\right), \\ X_{j(f+1)} &= X_{j(f)} + V_{j(f+1)}. \end{aligned} \tag{3}$$

$P_{\text{best}j}$ and $G_{\text{best}j}$ are the personal and global best positions of particle j, respectively; rand, w, c_1, and c_2 are the random number (from 0 to 1), the weighting function, the cognition, and social learning rate, respectively [29, 30].

The statistical random numbers that provide updated velocities in PSO may cause an uncontrollable gain in

Table 1: Process input factors and their levels.

S. no.	Coded factor	Parameters	Levels		
			1	2	3
1	P	Pulse-on-duration μs	25	35	50
2	Q	Pulse-off-duration μs	8	11	14
3	C	Maximum-current A	2	3	4
4	V	Voltage volts	40	45	50

Table 2: Experimental orthogonal array design and corresponding results.

P	Q	C	V	Material removal rate (mm^3/min)	Surface roughness (μm)
3	3	3	3	2.6296	2.394
3	3	3	1	2.65335	2.413
3	3	1	1	2.51275	1.52
3	1	1	3	3.3649	1.8145
3	3	1	3	2.73695	1.501
2	2	2	3	2.70275	2.28
2	2	2	2	2.7113	2.318
1	3	3	1	3.06945	2.584
1	1	3	1	3.4523	2.6125
3	2	2	2	2.64575	2.1185
2	3	2	2	2.508	2.204
2	1	2	2	2.62295	2.299
2	2	2	2	2.5916	2.318
1	2	2	2	2.8291	2.3275
2	2	2	2	2.7797	2.413
3	1	3	1	2.8196	2.508
2	2	2	2	2.78065	2.337
2	2	3	2	3.0761	2.546
1	1	3	3	3.1996	2.5935
1	1	1	1	3.25375	1.881
2	2	2	2	2.73125	2.318
2	2	2	2	2.6182	2.3275
2	2	1	2	3.11885	1.672
3	1	1	3	2.47665	1.596
2	2	2	1	2.70275	2.318
1	3	3	1	3.4694	1.786
1	3	3	3	3.5663	1.7575
3	1	3	1	2.40255	1.653
3	1	3	3	2.8196	2.489
1	3	3	3	2.8633	2.5745

velocity, as well as the search algorithm's uncertainty. This can be avoided by employing the Pareto front algorithm in conjunction with the genetic algorithm in a multiobjective PSO. Converging to the Pareto front for ideal global-optimized solutions group and supporting variation and scattering in solutions are two goals of the MOOPSO. In addition, the swarm/flock maintained their global best status. MOOPSO goes through the steps listed in Figure 1.

Instead of a single solution, multiobjective states produce an optimum set of solutions for input factors. They frequently incorporate opposing answers, such that one goal is improved while causing a reduction in solution. MOO can be accomplished in two ways: by combining each objective function into a single compound function or by changing the constraint group's response fully. The fundamental benefit of such a "weighted-sum" strategy is that it allows for both candid and quantitatively successful use. Establishing a complete Pareto-front-optimum solutions group or an illustrative subset is the second universal method. Non-dominated (ND) solutions are solutions that can improve any response by worsening one or more individual responses. The goal of running a MOO is to get a collection of ND solutions that stabilize the transaction amid completely different responses, which is known as a Pareto set. The proposed effort entails maximizing MRR while lowering SR.

3. Results and Discussion

3.1. Influence of Input Factors on Responses MRR and SR. The influence of various input factors on the responses (MRR and SR) was explored using ANOVA at the 0.05 level significant to identify the influence of various input factors on the responses (MRR and SR). ANOVA for MRR and SR (refer to Tables 3 and 4) with a small probability value suggests a higher correlation coefficient value. According to the RSM analysis, the quadratic model utilized for MRR and SR is statistically significant. When the "coefficient of determination" R^2 reaches 1, it signifies that the output features match the real data, and it also aids in determining whether the predicted and neighbouring R^2 (i.e., Pred-R^2 and Adj-R^2) have reached unity. R^2 and Adj-R^2 of both machining characteristics (MRR and SR) are above 90%, indicating that the regression-based mathematical model has a solid link between process parameters and output results. P, square terms-CxC, and interaction terms-PxC are determined to be the most significant inputs. For MRR, the process parameters V, Q, and C are shown to be unimportant. Similarly, the ANOVA table for SR reveals that the substantial process parameters are C, P, and Q, as well as the square term-CxC. For SR, V is shown to be a nonsignificant input factor.

As illustrated in Figure 2(a) for MRR and Figure 2(b) for SR, Pareto charts also display the most and least significant factors at the individual, square, and interaction levels of factors.

Figure 3 depicts a 3D surface plot of output MRR as a function of input factors, while Figures 3(a) to 3(f) depict the impact of P, Q, C, and V interactions on MRR. With higher C, the MRR lowers more, and with a pulse on time, it declines less. As a result, increasing C (from 2 to 4A) may significantly reduce the MRR without even increasing the pulse on time since it promotes rapid melting and alloy vaporization. However, the midrange value of C may improve MRR up to $P = 37.5\ \mu$s and then remain the same up to 45 μs, irrespective of P and C changes after 45 μs, because a high value of C directs a large amount of energy hooked on the targeted area to remove a higher amount of metal, as well as impulsive forces in the dielectric fluid, to take away molten metal from the targeted area. With a rise in C, the MRR also increases due to changes in form as well as the size of surface pits, pores, and other features, whereas factors Q and V have the opposite effect, contributing to the MRR value only if P and C are also changing. Figures 4(a) to 4(f) show the interactions of the input components on SR. Because low impulsive forces persist a longer duration when

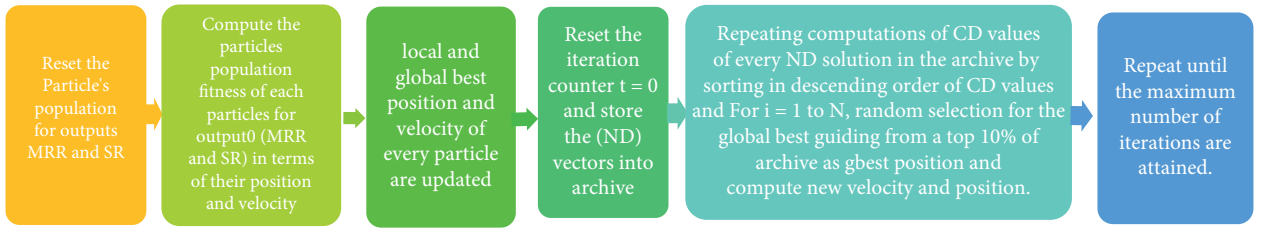

Figure 1: Steps involved in GA-PSO.

Table 3: ANOVA table for MRR.

Basis	Degree of freedom	Adjusted-sum of squares	Adjusted-mean squares	F value	P value	
Model	14	2.72112	0.19437	12.57	≤0.001	
Linear	4	1.53423	0.38356	24.81	≤0.001	
P	1	1.52466	1.52466	98.63	≤0.001	Significant
Q	1	0.00820	0.00820	0.53	0.478	
C	1	0.02251	0.02251	1.46	0.246	
V	1	0.00004	0.00004	0.00	0.960	
Square	4	0.91195	0.22799	14.75	≤0.001	
$P2$	1	0.00132	0.00132	0.09	0.774	
$Q2$	1	0.03858	0.03858	2.50	0.135	
$C2$	1	0.45050	0.45050	29.14	≤0.001	Significant
$V2$	1	0.00075	0.00075	0.05	0.828	
Two-way interaction	6	0.55061	0.09177	5.94	0.002	
$P \times Q$	1	0.00615	0.00615	0.40	0.538	
$P \times C$	1	0.24869	0.24869	16.09	0.001	Significant
$P \times V$	1	0.01557	0.01557	1.01	0.332	
$Q \times C$	1	0.21787	0.21787	14.09	0.002	
$Q \times V$	1	0.00302	0.00302	0.20	0.665	
$C \times V$	1	0.05957	0.05957	3.85	0.068	
Error	15	0.23187	0.01546			
Lack of fitness	10	0.19949	0.01995	3.08	0.113	
Fundamental error	5	0.03238	0.00648			
Total	29	2.95299				
R^2	92.15%	R^2 (adjusted)	90.82%	R^2 (predicted)	84.38%	

Table 4: Analysis of variance table for SR.

Basis	Degree of freedom	Adjusted-sum of squares	Adjusted-mean squares	F value	P value	
Model	14	3.64511	0.26037	149.83	≤0.001	
Linear	4	3.32368	0.83092	478.17	≤0.001	
P	1	0.15273	0.15273	87.89	≤0.001	Significant
Q	1	0.02758	0.02758	15.87	0.001	
C	1	2.98655	2.98655	1718.68	≤0.001	Significant
V	1	0.00457	0.00457	2.63	0.126	
Square	4	0.21599	0.05400	31.07	≤0.001	
$P2$	1	0.00365	0.00365	2.10	0.168	
$Q2$	1	0.00077	0.00077	0.44	0.516	
$C2$	1	0.06765	0.06765	38.93	≤0.001	Significant
V2	1	0.00248	0.00248	1.42	0.251	
Two-way interaction	6	0.01580	0.00263	1.52	0.239	
$P \times Q$	1	0.00290	0.00290	1.67	0.216	
$P \times C$	1	0.01064	0.01064	6.12	0.026	
$P \times D$	1	0.00003	0.00003	0.02	0.899	
$Q \times C$	1	0.00105	0.00105	0.60	0.449	
$Q \times V$	1	0.00006	0.00006	0.04	0.851	
$C \times V$	1	0.00085	0.00085	0.49	0.495	
Error	15	0.02607	0.00174			
Lack of fitness	10	0.01913	0.00191	1.38	0.380	
Fundamental error	5	0.00693	0.00139			
Total	29	3.67118				
R^2	99.29%	R^2 (adjusted)	98.63%	R^2 (predicted)	98.19%	

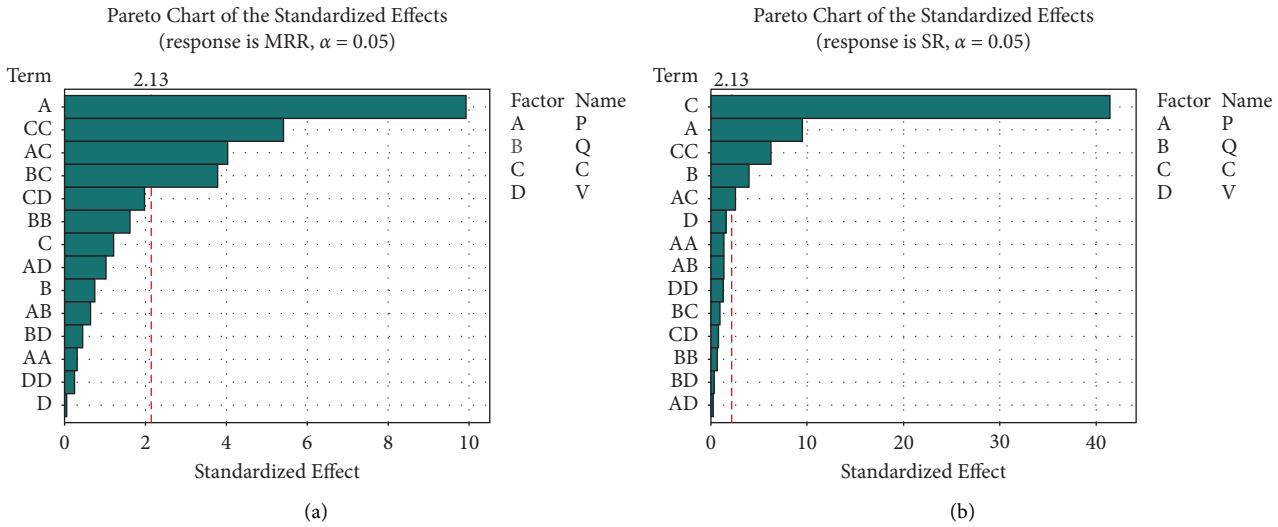

Figure 2: Pareto charts for input factors on the response (a) MRR and (b) SR.

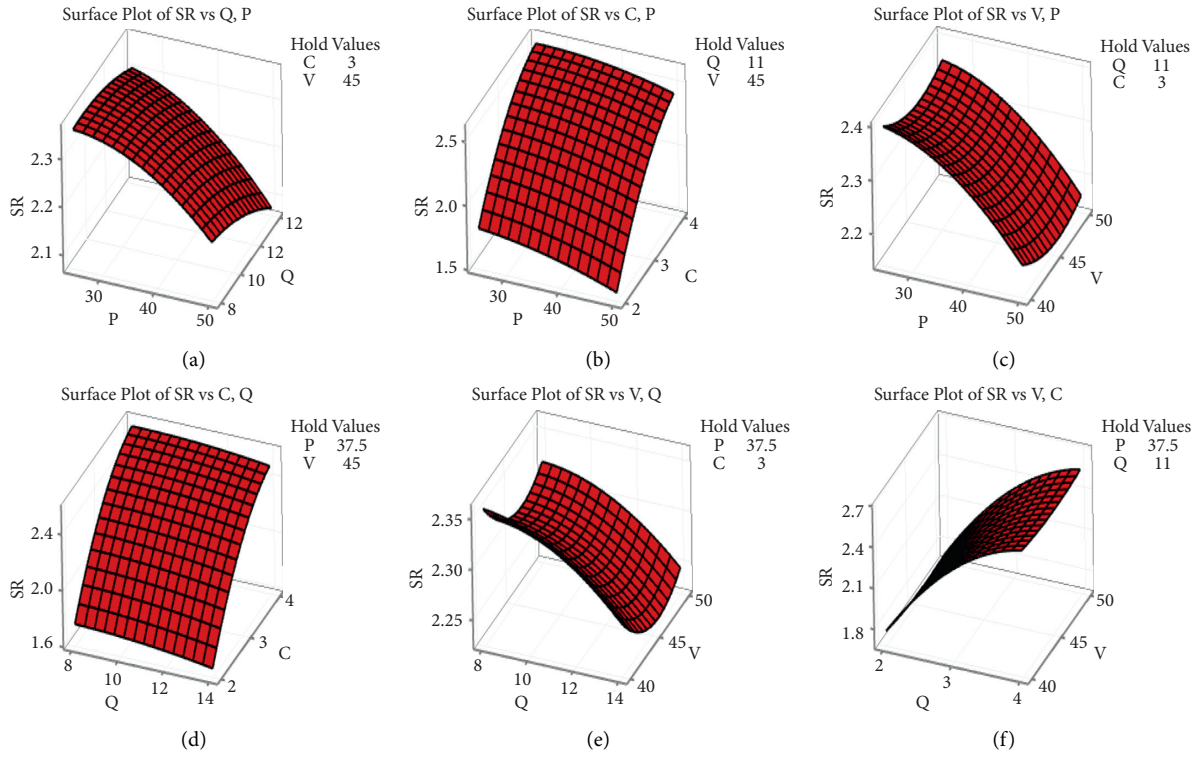

Figure 3: (a)–(f) The 3D contours of input factors on MRR.

C is low, SR decreases as *P* increases. However, as *C* rises, SR rises with it, because large impulsive forces, sparks, and retention for extended periods of time would damage the surface, and therefore SR rises. Because of the rapid rate of erosion of an alloy, pits and pores grow. Low thermal conductivity and melting point also contribute to a higher

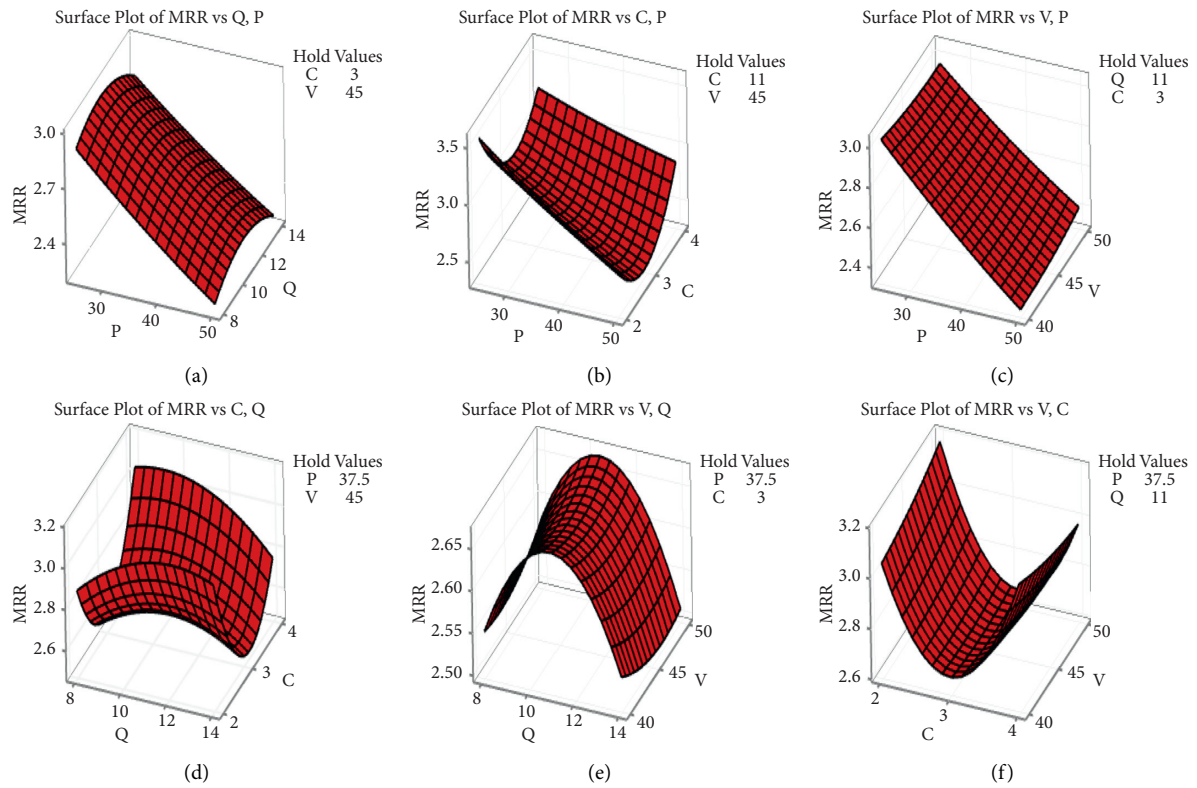

Figure 4: (a)–(f) The response of input attributes on SR.

SR [31]. In equations (4) and (5), the decisive empirical formed equations of machining characteristics (MRR and SR) are described.

$$\mathrm{MRR} = 6.30 - 0.0971 * P + 0.426 * Q - 1.923 * C - 0.033 * V + 0.000144 * P^2 - 0.01338 * Q^2 + 0.4116 * C^2 + 0.00067 * V^2 + 0.000548 * P * Q + 0.01060 * P * C + 0.000523 * P * V - 0.0390 * Q * C - 0.00094 * Q * V - 0.01224 * C * V, \tag{4}$$

$$\mathrm{SR} = 2.58 + 0.0067 * P + 0.0283 * Q + 1.195 * C - 0.1198 * V - 0.000240 * P^2 - 0.00189 * Q^2 - 0.1595 * C^2 + 0.00122 * V^2 - 0.000377 * P * Q + 0.002193 * P * C + 0.000023 * P * V + 0.00271 * Q * C + 0.000136 * Q * D + 0.00146 * C * V. \tag{5}$$

3.2. Multiresponse Optimization Using RSM. To maximize WEDM performance, the best factors must be chosen by considering responses like high MRR and low SR, which are hard to attain for a high-quality surface. The composite desirability (cd) approach is the most appropriate technique for optimizing input factors to satisfy response conditions using its function that determines the scale-free value (d_i) of the responses called desirability (lies between 0 and 1) expresses zero and absolute issues at their outer allowable margins. The weighted statistical average of the distinct desirability of responses is called cd. By integrating the objectives to satisfy the combined goals of all the responses, the optimum factors with the greatest desirability will be chosen for the mathematical models of MRR and SR.

By integrating the objectives to satisfy the combined goals of all the responses, the optimum factors with the greatest desirability will be chosen for the mathematical models of MRR and SR. Higher MRR and lower SR, as well as their expected optimum input factor values, are evaluated by the optimality solution, as shown in Table 5. The desirability does not have to be one, but its value reveals how close the margins on the true optimum values are. Table 6 shows the results of evaluating the best collection of factors using Minitab 19 software. Once the optimum values have been determined, it is essential to validate the results by conducting tests at these optimum values to ensure that they are correct. Table 5 shows the percent error for confirming the WEDM experimentation results, which

Table 5: Predicted and observed values of nitinol alloy.

Response		Observed	SE fit	Predicted		Error (%)
				95% CI	95% PI	
SR	Minimize	1.7618	0.0331	(1.6912, 1.8324)	(1.6484, 1.8753)	1.5
MRR	Maximize	3.5662	0.0988	(3.3556, 3.7767)	(3.2277, 3.9046)	2.5

Table 6: Optimum values of nitinol alloy.

Factors	P	Q	C	V
Levels	25	13.3861	2	48.5859

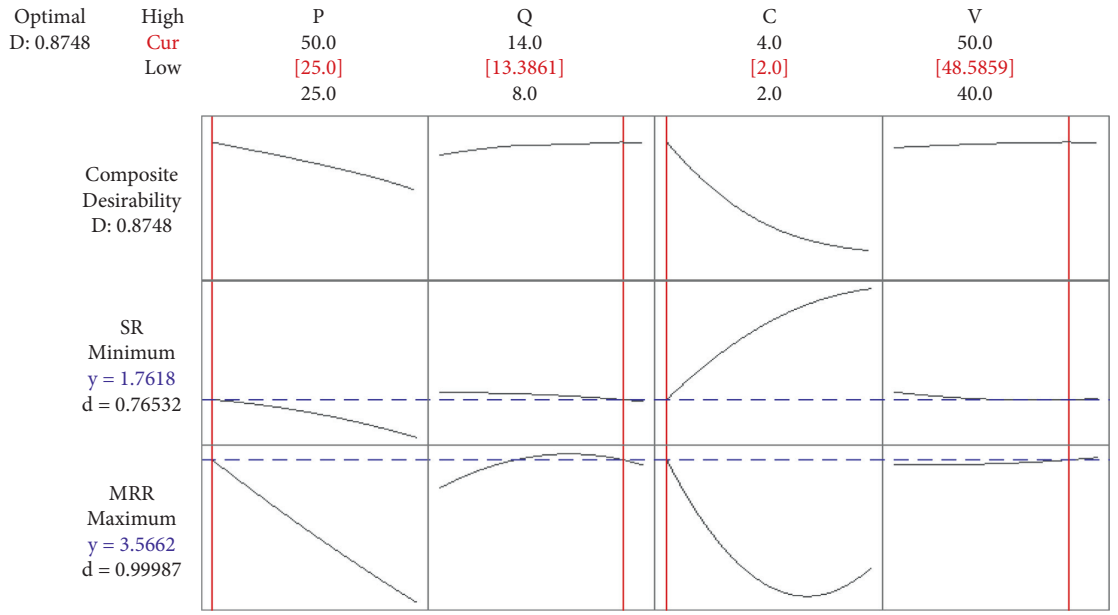

Figure 5: Desirability and optimal for input and responses.

the researchers determined to be very modest and acceptable.

The d_i value achieved for each response generated between low and high values is shown in the desirability gradient and a line graph of the WEDM process (refer to Figure 5). If the targeted responses d_i value is close to 1, then the desirability is high. The global desirability $D = 0.8748$ indicates that the responses are reasonably close to the target specified.

3.3. Results of MOOPSO. The PSO technique was applied with the understanding that neither should be minimized since when the SR is reduced by minimizing the objective function, the MRR is reduced as well. However, we need to maximize MRR while decreasing SR. An optimal collection of input factors must be found to minimize conflict between MRR and SR objectives and to obtain higher MRR and lower SR. As a result, the MRR objective function is changed to a minimization form as shown below:

Function 1 = minimize (1/MRR);

Function 2 = minimize (SR).

A PSO toolbox of the MATLAB software was used to execute the source code of the expected algorithm in order to achieve MO optimization as per specific goals. The Pareto front distribution contains 100 optimum sets of factors that satisfy both functions' conditions. Figure 6 depicts the Pareto front distribution of top-scored ND solutions from a collection of 100 best populations while optimizing two functions. The optimal option is determined by product requirements or an engineer's choice for a custom-designed procedure. Within the levels of factors, MOOPSO forecasted the best outcomes. Top-scoring solutions are selected from a pool of 100 global top solutions, but only the best 26 are presented in Table 7. The maximum value of 3.5420068 mm^3/min is found at pulse-on-duration of 25.1118229 μs, pulse-off-duration of 12.3503394 μs, C of 2.009124 A, and V of 45.120498 volts, corresponding to experiment no. 27 in Table 2 where the maximum MRR = 3.5663.23 mm^3/min at pulse-on-duration = 25 μs, $Q = 14\,\mu$s, $C = 14$ A, and $V = 50$ volts. The MRR of the Pareto front optimal solution shows values that are slightly lower

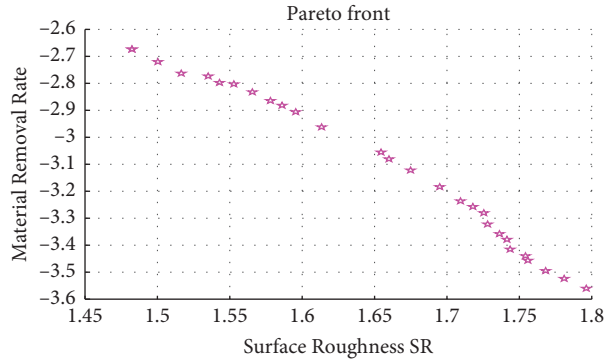

Figure 6: Pareto optimal front diagram of two responses using MOOPSO.

Table 7: Some of the Pareto front solutions of MOOPSO.

No.	P	Q	C	V	SR	MRR
1	25.1118229	12.3503394	2.009124	45.120498	1.7886815	3.5420068
2	26.3527045	13.5577625	2.005825	45.559656	1.7556562	3.46765
3	40.5901393	13.556345	2.005689	45.5593612	1.6270165	2.970345
4	44.2577660	13.623444	2.004210	45.6723322	1.5748247	2.85222
5	41.372580	13.632751	2.005639	45.504659	1.615188	2.94130952
6	25.139723	13.565896	2.007550	45.6149662	1.762997	3.5107027
7	29.943054	13.552877	2.000158	45.716168	1.727940	3.3438364
8	30.842303	13.568946	2.005914	45.455762	1.725763	3.3032148
9	47.516891	13.632021	2.007591	45.6219439	1.52834	2.74627547
10	39.339483	13.582901	2.007125	45.2547781	1.643595	3.0060108
11	28.36971	13.632919	2.00671	45.4713454	1.7426199	3.3889483
12	27.66276	13.560233	2.007347	45.6554528	1.748633	3.4182121
13	43.27807	12.983334	2.000026	45.2635824	1.6037521	2.8990178
14	49.83780	13.8012141	2.00763	45.500426	1.4855502	2.66760113
15	38.35412	13.464438	2.00110	45.554622	1.6526097	3.052191
16	35.93012	13.634225	2.00632	45.626082	1.67812964	3.12372824
17	38.680602	13.589088	2.00633	45.554353	1.64955087	3.03180880
18	47.918069	13.722225	2.007098	45.327659	1.51976365	2.72664270
19	45.3503468	13.475613	2.004385	45.4988402	1.56379364	2.81986745
20	46.4554287	13.740341	2.004998	45.460131	1.540144	2.7750993
21	32.6452667	13.6179144	2.007574	45.508611	1.710838	3.2359589
22	25.1265469	12.7423078	2.008351	45.2686245	1.780761	−3.5363104
23	26.8341290	13.5680084	2.005942	45.573252	1.752719	−3.4493672
23	48.2690753	13.7415251	2.007302	45.344606	1.513625	2.71524689
25	37.0194402	13.6473782	2.007617	45.4665371	1.6678021	3.08331782
26	37.2760105	13.5648563	2.006178	45.668391	1.6654667	3.08127597

than those of the experiment. Furthermore, the 3D MRR output plot (see Figure 3) shows that when the pulse on time and C grow, the MRR decreases. A better mix of input factor levels may result in a higher MRR value. In trials with s. no. 11 at pulse-on-duration = 35 μs, $Q = 14\,\mu$s, $C = 3$ amp, and $V = 45$ volts, a minimum MRR of 2.508 mm^3/min (refer to Table 2) was discovered. At pulse-on-duration = 49.83780 μs, $Q = 13.8012141\,\mu$s, $C = 2.00763$ A, and $V = 45.50042649$ volts, the Pareto front generated the lowest MRR of 2.66760113 mm^3/min. When comparing the minimal MRR, the experimental result is 0.13 mm^3/min greater, which is highly acceptable, and this variation is due to factor level changes.

Similarly, Pareto front findings revealed a minimum SR of 1.4855502 μm at $P = 4549.83780\,\mu$s, $Q = 13.801214\,\mu$s, $C = 2.00763$ A, and $V = 45.500426$ volts, whereas experiment output no. 5 (see Table 2) revealed a minimum SR of 1.501 μm at $P = 50\,\mu$s, $Q = 14\,\mu$s, $C = 2$ A, and $V = 50$ volts. Furthermore, the 3D response plots of SR (Figure 4) reveal that as P, V, and C increase, the SR decreases. As a result, the right quantities of input components provide the minimal SR, which is the hour's need. Furthermore, for $P = 25\,\mu$s, $Q = 8\,\mu$s, $C = 4$ A, and $V = 40$ volts, experimental output no. 9 had a maximum SR of 2.615 μm. While the highest SR of 1.7886815 μm was seen at $P = 25.1118229\,\mu$s, $Q = 12.3503394\,\mu$s, $C = 2.009124$ A, and $V = 45.1204989$ volts, the corresponding results of the Pareto front were seen with the maximum SR of 1.7886815 μm at $P = 25.1118229\,\mu$s, $Q = 12.3503394\,\mu$s, $C = 2.009124$ A, and $V = 45.12049$ volts. When comparing the maximum SR of experimental findings

Table 8: The best five optimum solutions of MOOPSO after confirmation test.

Run order	P	Q	C	V	SR	MRR
1	25.1118229	12.3503394	2.009124	45.120498	1.7886815	3.5420068
7	29.943054	13.552877	2.000158	45.716168	1.727940	3.3438364
9	47.516891	13.632021	2.007591	45.621944	1.52834	2.7462755
10	39.339483	13.582901	2.007125	45.254778	1.643595	3.0060108
14	49.83780	13.8012141	2.00763	45.500426	1.4855502	2.66760113

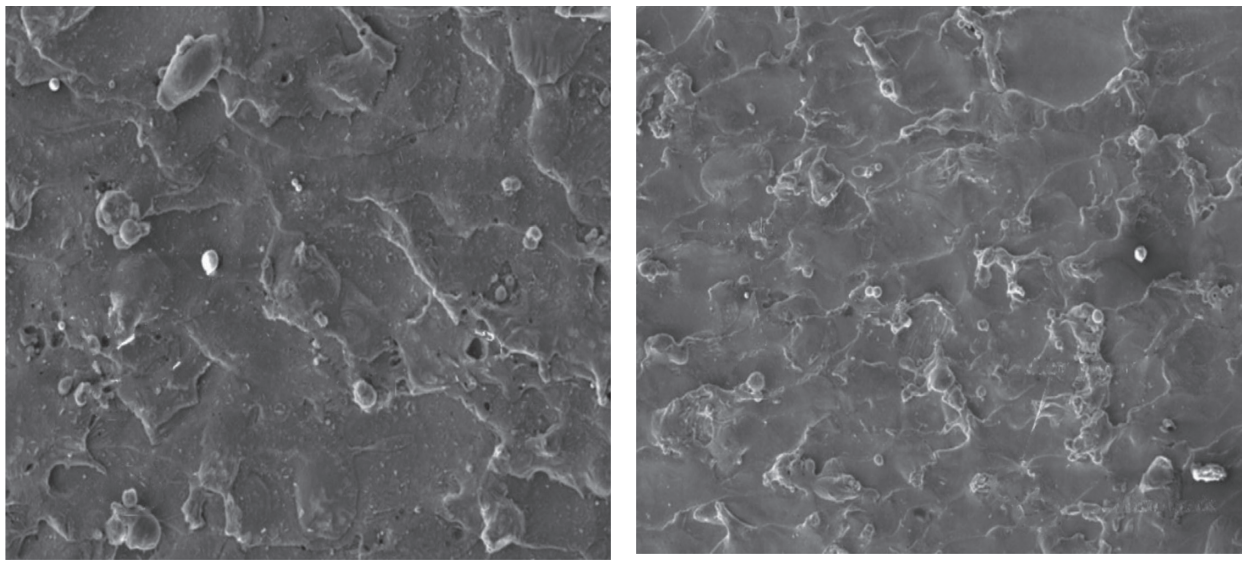

(a) (b)

Figure 7: SEM micrograph of the machined surface obtained (a) at high discharge energy level and (b) at optimized parameter.

to the Pareto optimum results, the experimental results are 0.4 μm higher. This could be due to changes in factor levels between the two approaches. Table 8 contains a list of the top five Pareto front solutions.

When the variables ($P = 50\,\mu$s, $Q = 14\,\mu$s, $C = 4$ A, and $V = 50$ volts) for the machined specimen (refer to Figure 7(a)) are set to high P, a large quantity of globules, micropores, and microcracks are produced, whereas, at an optimum combination of factors, SEM plots of the machined specimen (refer to Figure 7(b)) also create certain amounts of micropores, deposited film, some microcracks, and bead-shaped globules, because any setting of WEDM factors provides a low release energy level. As a result, these flaws cannot be totally eliminated. Input attribute optimization, on the other hand, has greatly decreased machining surface wear and tear, resulting in fewer fractures and flaws, as well as improved surface integrity. If molybdenum is not deposited, it can be reused, even at high release energies, to withstand enhanced chemical interactions between electrodes and dielectric fluid, resulting in a high MRR and increased productivity.

4. Conclusions

This research used particle swarm optimization (PSO) and RSM approaches based on a CCD experimental design for multiresponse optimization of input parameters in the WEDM method of nitinol alloy. Optimization was carried out using the composite desirability approach, resulting in an empirical model for analyzing the effect of input factors on multiresponses (MRR and SR). The following conclusions were drawn from the outcomes of several strategies for maximizing MRR and minimizing SR:

(1) P and C are substantially contributing elements on machining responses with maximization of MRR/minimization of SR, such that the minimum level of P and C discharge quick energy (electrical type) for alloy melting and vaporization. As impulsive forces created are of smaller intensity, this results in maximal MRR and least SR.

(2) The composite desirability approach for optimizing multiresponses yields the optimal combination for establishing the level of factors for high MRR and low SR with a very low percentage of error but acceptable: $P = 25\,\mu$s, $Q = 13.39\,\mu$s, $C = 2.0$ A, and $V = 48.59$ volts

(3) The response MRR increased, and SR decreased with decreasing P and C rather than Q and V in the MOOPSO Pareto front solution.

(4) In comparison to experimentation, the MOOPSO supplied a large combination of input factors,

allowing us to select extremely appropriate levels of factors to optimize MRR while minimizing SR to improve process efficiency.

(5) MOOPSO has been used to show which combinations of high and low levels P, Q, C, and V are best for the maximum and lowest of both responses (MRR and SR).

(6) The MOOPSO gave a collection of optimum solutions utilizing a Pareto optimal front to allow designers to select the best values of elements for their product requirements [32–34].

Data Availability

The data analyzed for this article are part of the authors' research work and are available for public use.

Disclosure

This paper was submitted as a presentation of the manuscript "Multi Response Particle Swarm Optimization of Wire-Electro-Discharge Machining Parameters of Nitinol Alloys" as preprint in the research square.

Conflicts of Interest

The authors declare that there are no potential conflicts of interest concerning research, authorship, and/or publication of this article.

Acknowledgments

The authors would like to thank the Deanship of Scientific Research at Umm Al-Qura University for supporting this work by Grant CODE: (20UQU072DSR).

References

[1] A. V. Srinivasan and D. M. McFarland, "Smart structures: analysis and design," *Measurement Science and Technology*, vol. 13, no. 9, pp. 1502-1503, 2002.

[2] H. C. Lin, K. M. Lin, and Y. C. Chen, "A study on the machining characteristics of TiNi shape memory alloys," *Journal of Materials Processing Technology*, vol. 105, no. 3, pp. 327–332, 2000.

[3] Y. S. Liao and Y. P. Yu, "Study of specific discharge energy in WEDM and its application," *International Journal of Machine Tools and Manufacture*, vol. 44, no. 12–13, pp. 1373–1380, 2004.

[4] O. A. A. Zeid, "On the effect of electrodischarge machining parameters on the fatigue life of AISI D6 tool steel," *Journal of Materials Processing Technology*, vol. 68, no. 1, pp. 27–32, 2002.

[5] M. A. E.-R. Merdan and R. D. Arnell, "The surface integrity of a die steel after electrodischarge machining: 2 residual stress distribution," *Surface Engineering*, vol. 7, no. 2, pp. 154–158, 1991.

[6] F. Han, J. Jiang, and Y. Dingwen, "Influence of discharge current on machined surfaces by thermo-analysis in finish cut of WEDM," *International Journal of Machine Tools and Manufacture*, vol. 47, no. 7–8, pp. 1187–1196, 2007.

[7] S. Narendranath, M. Manjaiah, S. Basavarajappa, and V. Gaitonde, "Experimental investigations on performance characteristics in wire electro discharge machining of Ti50Ni42.4Cu7.6 shape memory alloy," *Proceedings of the Institution of Mechanical Engineers - Part B: Journal of Engineering Manufacture*, vol. 227, no. 8, pp. 1180–1187, 2013.

[8] H. Soni, N. Narendranath, and M. Ramesh, "Effects of wire electro-discharge machining process parameters on the machined surface of Ti50Ni49Co1 shape memory alloy," *Siliconindia*, vol. 11, no. 2, pp. 733–739, 2018.

[9] A. Goswami and J. Kumar, "Investigation of surface integrity, material removal rate and wire wear ratio for WEDM of Nimonic 80A alloy using GRA and Taguchi method," *Engineering Science and Technology, an International Journal*, vol. 17, no. 4, pp. 173–184, 2014.

[10] A. Kumar, V. Kumar, and J. Kumar, "Multi-response optimization of process parameters based on response surface methodology for pure titanium using WEDM process," *International Journal of Advanced Manufacturing Technology*, vol. 68, no. 9–12, pp. 2645–2668, 2013.

[11] R. A. Laghari, L. Jianguang, X. Zhengyou, and S.-Q. Wang, "Modeling and optimization of tool wear and surface roughness in turning of austenitic stainless steel using response surface methodology," *3D research*, vol. 9, no. 3, pp. 1–13, Article ID 199, 2018.

[12] A. A. Khaled and S. Hosseini, "Fuzzy adaptive imperialist competitive algorithm for global optimization," *Neural Computing & Applications*, vol. 26, no. 4, pp. 813–825, 2015.

[13] M. P. Garg, A. Kumar, and C. K. Sahu, "Mathematical modeling and analysis of WEDM machining parameters of nickel-based super alloy using response surface methodology," *Sādhanā*, vol. 42, no. 6, pp. 981–1005, 2017.

[14] T. M. C. Jegan and D. Ravindran, "Electrochemical machining process parameter optimization using particle swarm optimization," *Australian Journal Of Mechanical Engineering, Computational Intelligence*, pp. 1–19, 2017.

[15] N. Chakala, P. S. Chandrabose, and C. S. P. Rao, "Optimisation of WEDM parameters on Nitinol alloy using RSM and desirability approach," *Australian Journal of Mechanical Engineering*, pp. 1–13, 2019.

[16] J. Kennedy and R. Eberhart, "Particle swarm optimization," in *Proceedings of the IEEE international conference on neural networks*, vol. 4, pp. 1942–1948, IEEE, Perth, Australia, November 1995.

[17] C. B. Kalayci and S. M. Gupta, "A particle swarm optimization algorithm with neighborhood-based mutation for sequence-dependent disassembly line balancing problem," *International Journal of Advanced Manufacturing Technology*, vol. 69, no. 1–4, pp. 197–209, 2013.

[18] Q. Jia and Y. Seo, "An improved particle swarm optimization for the resource-constrained project scheduling problem," *International Journal of Advanced Manufacturing Technology*, vol. 67, no. 9–12, pp. 2627–2638, 2013.

[19] A. R. Yildiz and K. N. Solanki, "Multi-objective optimization of vehicle crashworthiness using new particle swarm-based approach," *International Journal of Advanced Manufacturing Technology*, vol. 59, no. 1–4, pp. 367–376, 2012.

[20] C. Prakash, S. Singh, M. Singh et al., "Multi-objective optimization of MWCNT mixed electric discharge machining of Al–30SiCp MMC using particle swarm optimization," *Futuristic Composites, Materials Horizons: From Nature to Nanomaterials*, pp. 145–164, 2018.

[21] S. Sun and H. Lu, "Self-adaptive parameter control in genetic algorithms based on entropy and rules of nature for

combinatorial optimization problems," in *Proceedings of the 2019 IEEE Symposium Series on Computational Intelligence (SSCI)*, pp. 2721–2728, Xiamen, China, December 2019.

[22] Y. Zhang, D.-w. Gonga, X.-z. Gao, T. Tianc, and X.-y. Sun, "Binary differential evolution with self-learning for multi-objective feature selection," *Information Sciences*, vol. 507, pp. 67–85, 2021.

[23] Y. Xue, Y. Tang, X. Xu, J. Liang, and F. Neri, "Multi-objective feature selection with missing data in classification," *IEEE Transactions on Emerging Topics in Computational Intelligence*, pp. 1–10, 2021.

[24] X.-F. Song, Y. Zhang, Y.-N. Guo, X.-Y. Sun, and Y.-L. Wang, "Variable-size cooperative coevolutionary particle swarm optimization for feature selection on high-dimensional data," *IEEE Transactions on Evolutionary Computation*, vol. 24, no. 5, pp. 882–895, 2020.

[25] R. Magabe, N. Sharma, K. Gupta, and J. Paulo Davim, "Modeling and optimization of Wire-EDM parameters for machining of Ni55.8Ti shape memory alloy using hybrid approach of Taguchi and NSGA-II," *International Journal of Advanced Manufacturing Technology*, vol. 102, no. 5-8, pp. 1703–1717, 2019.

[26] D. Montgomery, "Guidelines for designing experiments," *Design and Analysis of Experiments*, Wiley, New York, NY, USA, 2008.

[27] S. K. Shihab, "Optimization of WEDM process parameters for machining of friction-stir-welded 5754 Aluminum alloy using box-behnken design of RSM," *Arabian Journal for Science and Engineering*, vol. 43, no. 9, pp. 5017–5027, 2018.

[28] R. K. Bhushan, "Optimization of cutting parameters for minimizing power consumption and maximizing tool life during machining of Al alloy SiC particle composites," *Journal of Cleaner Production*, vol. 39, pp. 242–254, 2013.

[29] M. Yunus and M. S. Alsoufi, "Multi-objective optimizations of mechanical characteristics of objects in computer aided SIS manufacturing process using empirical PSO algorithm," *Revista Română de Informatică şi Automatică*, vol. 30, no. 3, pp. 23–36, 2020.

[30] H. A. Ghulman and M. Yunus, "An application of a genetic algorithm based on Particle Swarm Optimization to a multiple responses problem arising in the Tube Hydroforming Process," *Revista Română de Informatică şi Automatică*, vol. 31, no. 3, pp. 15–30, 2021.

[31] S. L. Chen, S. F. Hsieh, H. C. Lin, M. H. Lin, and J. S. Huang, "Electrical discharge machining of a NiAlFe ternary shape memory alloy," *Journal of Alloys and Compounds*, vol. 464, no. 1–2, pp. 446–451, 2008.

[32] R. K. Bhushan, "Multiresponse optimization of Al alloy-SiC composite machining parameters for minimum tool wear and maximum metal removal rate," *Journal of Manufacturing Science and Engineering*, vol. 135, no. 2, Article ID 021013, 2013.

[33] V. ChittaranjanDas, "Response surface methodology and desirability approach to optimize EDM parameters," *International Journal of Hospitality Information Technology*, vol. 9, no. 4, pp. 393–406, 2016.

[34] N. Sharma, T. Raj, and K. K. Jangra, "Parameter optimization and experimental study on wire electrical discharge machining of porous Ni40Ti60 alloy," *Proceedings of the Institution of Mechanical Engineers - Part B: Journal of Engineering Manufacture*, vol. 231, no. 6, pp. 956–970, 2017.